NRC Research Press

ARTICLE

Biogeochemistry of U, Ni, and As in two meromictic pit lakes at the Cluff Lake uranium mine, northern Saskatchewan

Konstantin von Gunten, Tyler Warchola, Mark W. Donner, Manuel Cossio, Weiduo Hao, Christopher Boothman, Jonathan Lloyd, Tariq Siddique, Camille A. Partin, Shannon L. Flynn, Arden Rosaasen, Kurt O. Konhauser, and Daniel S. Alessi

Abstract: Open pits, which remain after uranium (U) mining operations cease, can form meromictic lakes that develop suitable conditions for the containment of dissolved and colloidal metals. In this study, the distribution and speciation of U, nickel (Ni), and arsenic (As) in the water column of two meromictic pit lakes was investigated at the decommissioned Cluff Lake mine in northern Saskatchewan. The 28 m deep and older D pit had a chemocline at a 13 m depth, below which it turned anoxic and its meromixis was controlled by iron (Fe) cycling. Below the chemocline both Fe(III) and As(V) were reduced to Fe(II) and As(III), respectively. Iron cycling had a large effect on U distribution because reducing conditions prevented sulfide oxidation and a drop in pH in deeper layers. Metal-reducing bacteria were found to be present at, and below, the chemocline. In the deeper (90 m), larger and more recently flooded DJX pit, two chemoclines were observed at depths of 15 and 65 m. Both were linked to sharp U and Ni concentration gradients. Unlike the D pit, a transition to reducing conditions was not observed in the DJX pit's water column. However, colloidal U, primarily associated with aluminum oxyhydroxides, was found below the first chemocline. Overall, the meromixis type determined the distribution and speciation of metals and bacteria in the investigated pit lakes, thus providing insights into the use of pit lakes as a potential bioremediation strategy.

Résumé : Les cavités subsistantes après l'extraction d'uranium (U) forment souvent des lacs méromictiques contaminés avec des métaux. La distribution et la spéciation de U, nickel (Ni) et arsenic (As) a été étudiée dans deux lacs méromictiques à Cluff Lake, une mine au nord du Saskatchewan. Le lac D pit (28 m) était plus âgé et possédait une chimiocline à 13 m, sous laquelle il devenait anaérobique, cette stratification étant contrôlée par le fer (Fe), qui, ainsi que le As changeait de spéciation sous cette limite. Le cycle du Fe influençait la distribution de U et les conditions réduites sous la chimiocline prévenaient d'une chute du pH. Des bactéries réductrices de métaux ont été trouvées au niveau et sous la chimiocline. Dans le plus grand lac, DJX pit (90 m), se trouvait deux chimioclines (15 m et 65 m). Les deux étaient concomitantes à de forts gradients de concentrations de U et de Ni. Contrairement au D-pit, aucune transition redox n'a été observée, mais des colloïdes transportant de l'uranium principalement lié avec des oxyhydroxides d'aluminium ont pu être mis en évidence sous la première chimiocline. La méromicticité et les conditions d'oxydo-réductions contrôlaient donc la distribution et la spéciation des métaux et métalloïdes, ainsi que des bactéries. Ils offrent de nouveaux aperçus de l'utilisation des lacs méromictics pour la bioremédiation.

1. Introduction

1.1. Objectives

Canada is one of the largest uranium (U) producers in the world. The U mining process exposes excavated rock to surface oxidizing conditions, which can result in the mobilization and accumulation of metals and metalloids in nearby environments. Knowledge of the geochemical processes and reactions of potential contaminants at former mine sites is important to mitigate impacts from future mining operations. Despite the significant literature pertaining to U transport and bioremediation in laboratory studies and temperate field environments, such as the Rifle site in Colorado (Williams et al. 2011; Bargar et al. 2013; Alessi et al. 2014) and the Oak Ridge site in Tennessee (Watson et al. 2013; Leigh et al. 2015), little is known about the transport and fate of U in subarctic regions, such as those where Canada's U resources are mined. Arsenic (As) and nickel (Ni) are often found to be associated with U deposits and can become major contaminants in mining districts (Donahue et al. 2000). Accordingly, our motivation was to study U, Ni, and As mobility and speciation in two chemically stratified (meromictic) pit lakes in a subarctic climate at the decommissioned Cluff Lake mine, located in the Athabasca Basin in northern Saskatchewan (Fig. 1). These lakes are two examples of mine pit lakes with different histories, sizes, geometries, stratification behaviors, and U, Ni, and As metal distributions. Additionally, this study investigates the role of colloidal particles in the geochemical cycling of those metals.

Received 3 July 2017. Accepted 21 February 2018.

Paper handled by Associate Editor David Widory.

K. von Gunten, T. Warchola, M. Cossio, W. Hao, S.L. Flynn, K.O. Konhauser, and D.S. Alessi. Department of Earth and Atmospheric Sciences, University of Alberta, 1-26 Earth Sciences Building, Edmonton, T6G 2R3, Canada.
M.W. Donner and T. Siddique. Department of Renewable Resources, University of Alberta, 751 General Services Building, Edmonton, AB T6G 2H1, Canada.
C. Boothman and J. Lloyd. School of Earth and Environmental Sciences, University of Manchester, Oxford Road, Manchester, M13 9PL, United Kingdom.
C.A. Partin. Department of Geological Sciences, University of Saskatchewan, 114 Science Place, Saskatoon, SK S7N 5E2, Canada.
A. Rosaasen. AREVA Resources Canada, 817 45 St W, Saskatoon, SK S7K 3X5, Canada.
Corresponding author: Konstantin von Gunten (email: vongunte@ualberta.ca).

Fig. 1. (Left) The Athabasca Basin (light shape), the Carswell Structure (dark round shape), and the location of the former Cluff Lake uranium mine (mining symbol). (Right) The mining area with the meromictic pit lakes (D pit and DJN/DJX pits). For a more detailed map and corresponding geochemical data see Fig. S1[1] and Table S1[1] in the supplementary information. GIS data provided by AREVA. [Colour online.]

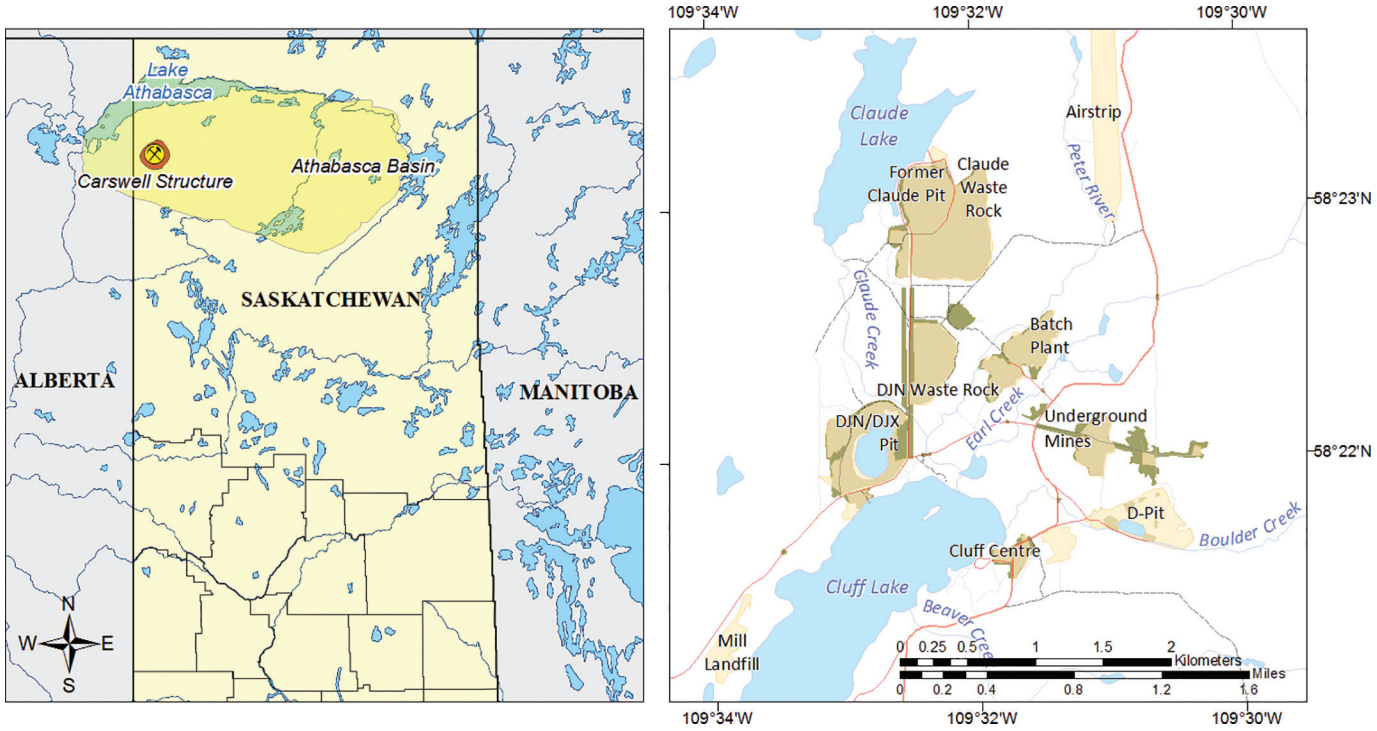

1.2. Geological setting

Cluff Lake is located in Canada's most important uranium mining region, the Paleo- and Mesoproterozoic Athabasca Basin, which contains the highest grade U deposits in the world (Donahue et al. 2000) (Fig. 1). The Athabasca Basin deposits are hosted in either crystalline basement rocks or within the overlying sandstone of the Athabasca Group (Kyser and Cuney 2008). The basement orthogneisses at the Cluff Lake site were exposed during the formation of the Carswell structure in the Paleozoic (Harper 1981). The U is predominantly found as uraninite–sulfide (dated at ~1150 Ma), uraninite–Te–Se–Bi (~1050 Ma), pitchblende–sulfide, and pitchblende–hematite (both ~380 Ma) (Bell 1985; Ruhlmann 1985). The ore found in the Athabasca Basin contains high grades of Ni (up to 2%) and As (up to 1.2%) due to the presence of primary minerals gersdorffite, niccolite, bravoite, and chalcopyrite (Donahue et al. 2000).

1.3. Characteristics of the pit lakes: D pit and DJX pit

In this study, we focused on two pit lakes at the Cluff Lake site (Fig. 1): D pit (formed 34 years ago) and DJX pit (formed 15 years ago). Mining of D pit occurred between 1979 and 1981 (AREVA 2009), during which time the nearby Boulder Creek was diverted to allow for pit development. In 1983 the creek overflowed during spring thaw and flooded the D pit (AREVA 2009). A waste rock pile located adjacent to the pit was revegetated between 1983 and 1985, but minor metal leaching from the covered waste pile has been reported (AREVA 2009). The D pit lake has a surface area of 15 400 m^2 and an approximate depth of 28 m.

The DJX pit was composed of two open pits: DJN Pit, which was mined from 1989 to 1991, and DJX pit, mined from 1994 to 1997. To develop the DJN Pit, the adjacent Claude Creek was diverted into the nearby Peter River. The DJN Pit was subsequently used for waste rock disposal (containing <0.03% U) from the adjacent DJX pit, which showed high potential for acid generation (AREVA 2009). After mining ceased in the DJX pit, it was seasonally dewatered to minimize water inflow to the nearby DJ underground mine (1994–2002). With the cessation of mining, the DJN pit and the DJX pit were flooded with water from the adjacent Cluff Lake (AREVA 2009), and today they form one water body, which will hereafter be referred to as DJX pit. The water level in the 90 m deep pit has stabilized below the level of nearby Cluff Lake, forming a pit lake with a surface area of approximately 85 900 m^2 (AREVA 2013).

Additional information on hydrology and climate, as well as the extent of the Cluff Lake mine areas and on historical sampling records can be found in Section 1 of the supplementary information (SI[1]). Relevant information on U biogeochemistry can be found in Section 2 of the SI[1].

1.4. Importance of colloids and meromixis

When metal speciation in natural environments is studied, it is important to consider that metals are often associated with colloidal particles between 1 nm and 1 μm in size (Dai et al. 1995). Colloids can play an important role at abandoned mining sites, as the revegetation of such areas can increase the abundance of low molecular weight acids that can interact with Fe-, Al-, and Si-bearing phases in soils and enhance colloid formation (Slowey et al. 2007). Such colloids can consist of organic carbon or oxyhydroxide aggregates containing Fe, Al, Si, or P, and crucially, they can increase the transport of metals under conditions that typically inhibit mobility (Dai et al. 1995; Kretzschmar and Schäfer 2005; Wang et al. 2013).

In general, when U ore is extracted from open pit mines, the mine pits can eventually fill with surface runoff (e.g., spring melt), rain-, and groundwater, forming pit lakes. A characteristic feature of these pit lakes are the steeply sided walls and considerable depth (Schultze et al. 2016). Relative depth is often calculated for

[1]Supplementary data are available with the article through the journal Web site at http://nrcresearchpress.com/doi/suppl/10.1139/cjes-2017-0149.

pit lakes, which is defined as the ratio of the maximum depth to the circular diameter of the surface (Pieters and Lawrence 2014). Such lakes can become meromictic, whereby the water body is separated by a chemocline into an upper mixolimnion that expresses seasonal turnover and a lower monimolimnion with limited water exchange with the overlaying water mass. These layers vary considerably in density and chemical composition. The formation of meromixis depends on various factors in addition to the shape of the lake basin including protection against wind, climatic conditions, ice melt and runoff, and groundwater inputs (Pieters and Lawrence 2014; Schultze et al. 2016; Boehrer et al. 2017). Meromixis is not always a stable condition; the regular mixing of the mixolimnion can push the chemocline down, whereas the turnover of the monimolimnion, initiated by the input of less saline groundwater or geothermal heating, can lead to its rise (Pieters and Lawrence 2014). The selective manipulation of the meromixis stability can be used as a pit lake remediation tool and has been applied for the containment of highly contaminated brines and acid mine drainage (Geller et al. 2012). Nevertheless, published meromixis related geochemical data are scarce and not all geochemical relations are well understood (Schultze et al. 2016).

2. Materials and methods

2.1. Water sampling and measurement of field parameters

In June 2016, water was sampled from D pit and DJX pit from a boat in the center of the pit. A plastic tube was lowered into the pit together with a measuring tape and the probe of a multiparameter water quality meter (Professional Plus, YSI, Rye Brook, New York). D pit was sampled from 0.5–23 m in 1 m intervals, whereas DJX pit was sampled from 0.5–82 m in 2–5 m intervals. Temperature, pH, oxidation-reduction potential (ORP), dissolved oxygen, and conductivity were recorded using the water quality meter at each depth. Sampled water was pumped through the tubing using a MasterFlex E/S portable sampler (Cole-Parmer, Vernon Hills, Illinois) and collected in the boat.

For metal quantification and arsenic speciation analysis, the water was filtered (0.45 μm nylon membranes, Agilent Technologies, Santa Clara, California) and collected into acidified (0.05 M HCl) 50 mL polypropylene tubes (Fisher Scientific, Pittsburgh, Pennsylvania), which were wrapped in aluminum foil to prevent photooxidation of redox-sensitive species. For carbon, nitrogen, and anion analyses, unfiltered water samples were collected without acidification. Separate nonacidified samples, filtered through 0.45 μm membranes, were collected into 250 mL polypropylene copolymer centrifuge bottles (Thermo Fisher, Waltham, Massachusetts), wrapped in aluminum foil, for asymmetrical flow field – flow fractionation. For iron speciation, 1 mL of water was directly filtered (0.45 μm) into 2 mL Eppendorf tubes and acidified with 1 mL of 2 M HCl for preservation. Results, collected in June 2016, were compared with preliminary field measurements (temperature, pH, conductivity) and water analyses (selected depths for cations, anions, carbon, and nitrogen, only) conducted in September of 2015 using similar methods (exception: 0.2 μm filters used). Field measurements for DJX pit were also performed in September 2016. Groundwater was sampled in June 2016 from wells located close to the two investigated pits (Fig. S1[1]). The well south of D pit was DWW0041G (7 m deep, N 58.3617°, W 109.5154°) and will hereafter be referred to as groundwater well 1 (GW1). Two groundwater wells close to the DJX pit were sampled: the well north of the DJX pit (GW2) is labeled as MNW6210G (17 m deep, N 58.3709°, W 109.5494°) and the well west of the DJX pit (GW3) is labeled as HYD9846AG (4 m deep, N 58.3675°, W 109.5489°). Three well volumes were pumped to adequately purge the well before sampling (Vai, 2013).

2.2. Water chemistry

The unfiltered and unacidified water samples were analyzed for total carbon, total inorganic carbon, and total nitrogen (TN) using a TOCV-N CHS/SCN Model Total Organic Carbon Analyzer (Shimadzu, Kyoto, Japan) with potassium nitrate and potassium hydrogen phthalate as calibration standards, and potassium acid phthalate certified reference material for quality control (detection limit: 0.1 parts per million (ppm)). Total organic carbon was calculated by determining the difference between total carbon and total inorganic carbon. Splits of the same samples were filtered (0.45 μm) for anion analysis by ion chromatography using a DX 600 (Dionex, Sunnyvale, California) with a 4 mm analytical column AS9-HC and a guard column AG9-HC (detection limit: 0.2–1.0 ppm). Filtered and acidified water samples were analyzed with an inductively coupled plasma mass spectrometer (ICP-MS/MS) triple quadrupole system (Agilent Technologies 8800). Single-element standards (Spex CertiPrep, Metuchen, New Jersey; Ricca Chemical Company, Arlington, Texas) were diluted in 2% HNO_3 (trace metal grade, Fisher Scientific) and 0.5% HCl (trace metal grade, Fisher Scientific) and used for external calibration. See SI, Table S2[1] for all used analyte masses and MS/MS modes.

2.3. Speciation of metals and metalloids

Selected samples (filtered, preserved in 1 M HCl) from both pits were subjected to a standard ferrozine assay based on the methods of Stookey (1970), Viollier et al. (2000), and Porsch and Kappler (2011) to determine iron speciation. Total Fe content was determined by adding 400 μL of hydroxylamine hydrochloride (10% in 1 M HCl) to 100 μL of each sample (preserved in 1 M HCl), which were left for 30 min in the dark. Then, 500 μL of ferrozine (0.1% in 50% ammonium acetate) were added, followed by another 5 min of incubation in the dark. Fe(II) concentrations were determined by adding 400 μL of 1 M HCl to 100 μL of each sample, followed by 500 μL of ferrozine. After 5 min of incubation time in the dark, the samples were analyzed on the spectrophotometer. The ferrozine complex was quantified spectrophotometrically at 562 nm using an Evolution 60S UV-Vis Spectrophotometer (Thermo Scientific). Calibration curves for total Fe and Fe(II) (0 to 1000 μM) were generated using $(NH_4)_2Fe(SO_4)_2{\cdot}6H_2O$ in 1 M HCl and confirmed by ICP-MS/MS.

Filtered and acidified samples were analyzed using a high-performance ion chromatograph (IC; Thermo Scientific Dionex ICS–5000$^+$) paired with a quadrupole inductively coupled plasma mass spectrometer (iCAP Q ICP-MS, Thermo Scientific) operated in kinetic energy discrimination mode with helium as the collision gas. Arsenic species were separated using a Dionex Ion Pac AS7 anion exchange column (4 mm inner diameter × 250 mm length) and AG7 guard column (4 mm inner diameter × 50 mm length), with dilute HNO_3 as the mobile phase. Samples were also analyzed for total concentrations of trace metals using an iCAP Q ICP-MS. More detailed method information can be found in Donner et al. (2017). Thermodynamic modeling of metal speciation was conducted using the PHREEQC 3.3.7 software (USGS, Reston, Virginia) and the Minteq (version 2009) database. Modeling was done for D pit at depths of 0.5 m, 5 m, 10 m, 13 m, and 20 m, and for DJX pit at 0.5 m, 50 m, and 80 m. For the inputs, measured cation and anion concentrations (in mol/L), pH, and ORP values were used (see SI, Table S11[1] for more details).

2.4. Asymmetrical flow field – flow fractionation

Filtered water samples collected for colloidal analysis were analyzed for the distribution of metals in the dissolved and colloidal (oxyhydroxides and organic matter) fractions. The analysis was completed using asymmetrical flow field – flow fractionation equipped with an auto injector (AF200 and PN5300, respectively, Postnova Analytics, Salt Lake City, Utah), coupled to a UV-visible absorbance detector (G4212 DAD, Agilent Technologies) and an iCAP Q ICP-MS (Thermo Scientific). The asymmetrical flow field – flow fraction-

Fig. 2. Schematic cross-section through the DJX pit (information provided by AREVA) and D pit (rough estimation) showing the 3 different water layers in each pit. For comparison, the relative vertical positions and dimensions of the groundwater wells, GW1 and GW2, are shown. The orientation of the cross-sections is shown at the bottom. Vertical exaggeration is 6.5 times. The curved blue arrows indicate potential groundwater inflow pathways. See Fig. S12[1] for a 3-D DJX pit model and for spatial location of GW2. [Colour online.]

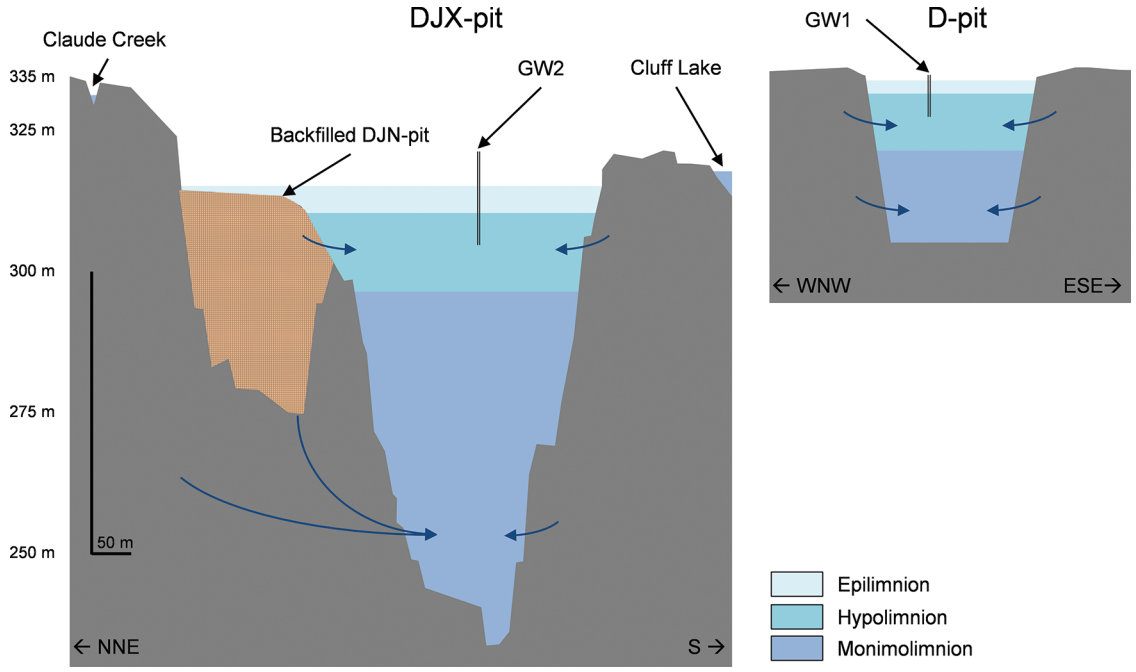

ation procedure is described elsewhere (Guéguen and Cuss 2011). Ultrapure water and HCl were used to adjust the pH and conductivity of the ultrapure ammonium carbonate carrier fluid buffer (Sigma-Aldrich, St. Louis, Missouri) to match the properties of the analyzed samples. Specifically, these adjustments were pH 7 and a conductivity of 300 μS/cm for D pit and DJX pit surface samples and pH 6 and 1500 μS/cm for DJX pit deep-water samples based on Neubauer et al. (2013). The areas of the free, organic matter-associated, and oxyhydroxide-associated peaks were determined using statistical deconvolution as described in Cuss and Guéguen (2012).

2.5. 16S-rRNA gene profiling

Prokaryotic diversity in the pit lakes was determined using 16S rRNA gene sequencing on selected unfiltered water samples from September 2015. DNA was extracted from the water samples using the PowerWater DNA Isolation Kit (Mobio, Carlsbad, California). Fifteen millilitres of each water sample were filtered through 0.2 μm membranes using a vacuum unit and the membranes were processed according to kit instructions. Sequencing was performed by a dual-index paired-end sequencing approach on an Illumina MiSeq sequencer based on the method by Kozich et al. (2013). Postprocessing was done using a pipeline consisting of the following applications: Cutadapt and FastQC (quality control), Sickle (quality trimming), SPADes (Illumina MiSeq errors correction), Pandaseq (merging of paired reads), Qiime with UPARSE and Vsearch (removal of singletons and chimeras, building of OTU tables and phylogenetic trees, and for Shannon diversity).

3. Results

3.1. Limnology of D pit and DJX pit

Schematic diagrams of D pit and DJX pit can be seen in Fig. 2 and are useful for understanding the different scales of the two locations. In September 2015, D pit expressed one thermocline around 5 m and one major halocline between 12–13 m, accompanied by a pH decrease from 8.1 to 7.8 (Fig. 3, left column). In June 2016, D pit expressed a similar halocline at 12–15 m depth. Between 2 and 12 m depth a pH decrease from pH 7.3 to 6.2 was recorded. The dissolved oxygen concentrations in D pit increased slightly within the first 2 m, decreased rapidly between 2 and 5 m, and then continued to decrease at a less rapid rate between 5–10 m. Corresponding to the oxygen curve, the ORP dropped from +200 mV (oxic conditions) to –300 mV (reducing conditions) between 12 and 20 m of depth. In this case, the upper 15 m can be referred to as mixolimnion, which by definition is affected by seasonal mixing.

The DJX pit showed a thermocline between 0 and 10 m in all data sets (Fig. 3, right column). In June 2016, the depth of the thermocline was similar to September 2015 but was associated with a stronger temperature gradient. Across all data sets, four haloclines were identified around the following depths: 5 m, 17 m, 55 m, and 65 m. The halocline at 5 m depth was closely associated with an increase in oxygen (e.g., up to 11.6 mg/L in June 2016), likely due to primary production, which was followed by an oxygen decline to 20 m (as low as 4.4 mg/L) and a more moderate decline to the bottom (<0.9 mg/L). The pH was generally lower than in D pit and decreased from pH 7.5 at 5 m depth to pH 5.5 below the halocline at 17 m depth. In the DJX pit, the ORP was positive throughout the measured column (150–280 mV), which may result from redox interactions, (e.g., by Mn(III/IV), NO_3^- (Schüring et al. 2013), or even sulfate), because under low pH conditions, sulfate-reducing environments might result in higher measured ORP values (Church et al. 2007, Falagán et al. 2013).

3.2. Distribution of metals and ligands

In the D pit, total carbon was 22 ppm at the surface, rising to 47 ppm at 17 m (Fig. 4, left column and Table S7[1]). It was dominated by inorganic species; organic carbon remained between 4 and 13 ppm. No phosphate was detected in D pit, likely due to precipitation with Fe (Jaeger 1994). Sulfate was detectable above 13 m, coinciding with the depth of the halocline and the change of the ORP from positive to negative. Below this depth, no SO_4^{2-} or NO_3^- could be detected; however, N was present, indicating that more reduced nitrogen species are present. The reduction of SO_4^{2-} can result in the precipitation of iron sulfide phases with low

Fig. 3. Limnological results (temperature, pH, specific conductivity, dissolved oxygen, and oxidative-reductive potential (ORP)) for D pit (left) and DJX pit (right) measured at the Cluff Lake site. Note the differences in depth (vertical scale) between the two pits. [Colour online.]

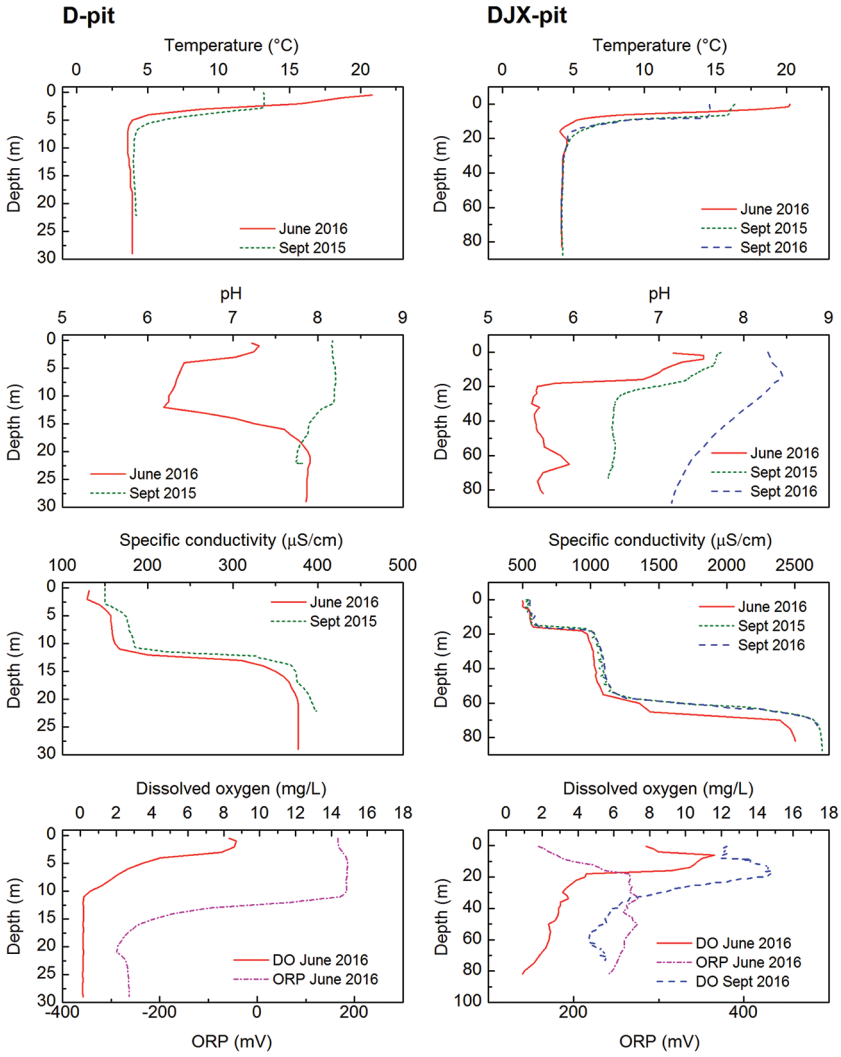

solubility, forming in the presence of Fe^{2+} and the negative ORP below the chemocline (Sobolewski 1999). In the D pit, concentrations of B, Na, Mg, K, Ca, Mn, and Fe increased with depth (Fig. 4, left column and Table S5[1]). A significant increase in Fe concentrations was observed below 12 m depth, coinciding with a drop in ORP values and oxygen concentrations. This suggests that there was a shift towards Fe(III)-reducing conditions, as supported by the Fe speciation results discussed below. Further, Mn concentrations steadily increased from 0.2 ppm to 3.3 ppm. Nickel concentrations were low at the surface of the D pit, with a concentration maximum of 9 parts per billion (ppb) measured at the chemocline; Ni then became undetectable below 15 m (Fig. 4, left column). The As concentration profile was similar to that of Fe, with the former increasing in concentration with depth from 2 ppb to 91 ppb and showing a small decrease at 20 m (76 ppb). The concentration profile of U was strongly linked to changes in pH. The drop to pH 6.2 between 4 and 12 m was associated with a decrease in U concentrations from 120 ppb at the surface to 64 ppb at 7 m depth. Below 11 m, U concentrations increased with increasing pH to 131 ppb (13 m) and stabilized below 16 m to around 90 ppb. A similar concentration trend was observed for Si (Table S5[1]).

In the DJX pit, total carbon ranged from 5.4 to 13.8 mg/L (Fig. 4, right column and Table S8[1]). DJX pit carbon composition was similarly dominated by inorganic carbon; however, this trend reversed after 70 m, where the presence of organic carbon became more predominant. Total organic carbon was generally lower in deeper water layers of the DJX pit compared with the D pit, in conjunction with the presence of oxygen. Sulfate-S values reached 78 mg/L at the 15 m halocline, up to 172 mg/L in the upper monimolimnion, and up to 476 mg/L near the bottom of the pit (82 m). Trace amounts of Se, V, Cd, Pb, Sb, and Tl were detected by iCAP Q ICP-MS (Table S12[1]). The deep water of DJX pit was rich in B, Na, Mg, K, Ca (dominant metal), and Mn, but depleted in Fe compared to the D-pit (Fig. 4, right column and Table S6[1]). This pattern was likely due to the presence of oxygen in the deep-water layers of DJX pit, leading to the precipitation of Fe(III) oxyhydroxides. Concentration curves of U, Ni, and Mn had similar shapes, with the two major chemoclines evident at 15 m and 65 m (Fig. 4, right column). Based on the high Mn concentrations, the bottom water layers of DJX pit were potentially in the redox transition zone between oxic and Mn(IV)-reducing conditions.

In general, the DJX pit metal concentration profiles indicate that stratification is an important control for metal distribution. A slight decrease was observed in the concentrations of U, Ni, and Zn (also Cu, as shown in Table S6[1]), which could indicate the beginning of the development of an anoxic zone below 82 m, where those metals might be precipitating as sulfides. Supporting this conclusion are the trace amounts of As at 80 m depth, which

Fig. 4. Measured cations, anions, carbon, and nitrogen in the D pit (left) and the DJX pit (right) in June 2016. [Colour online.]

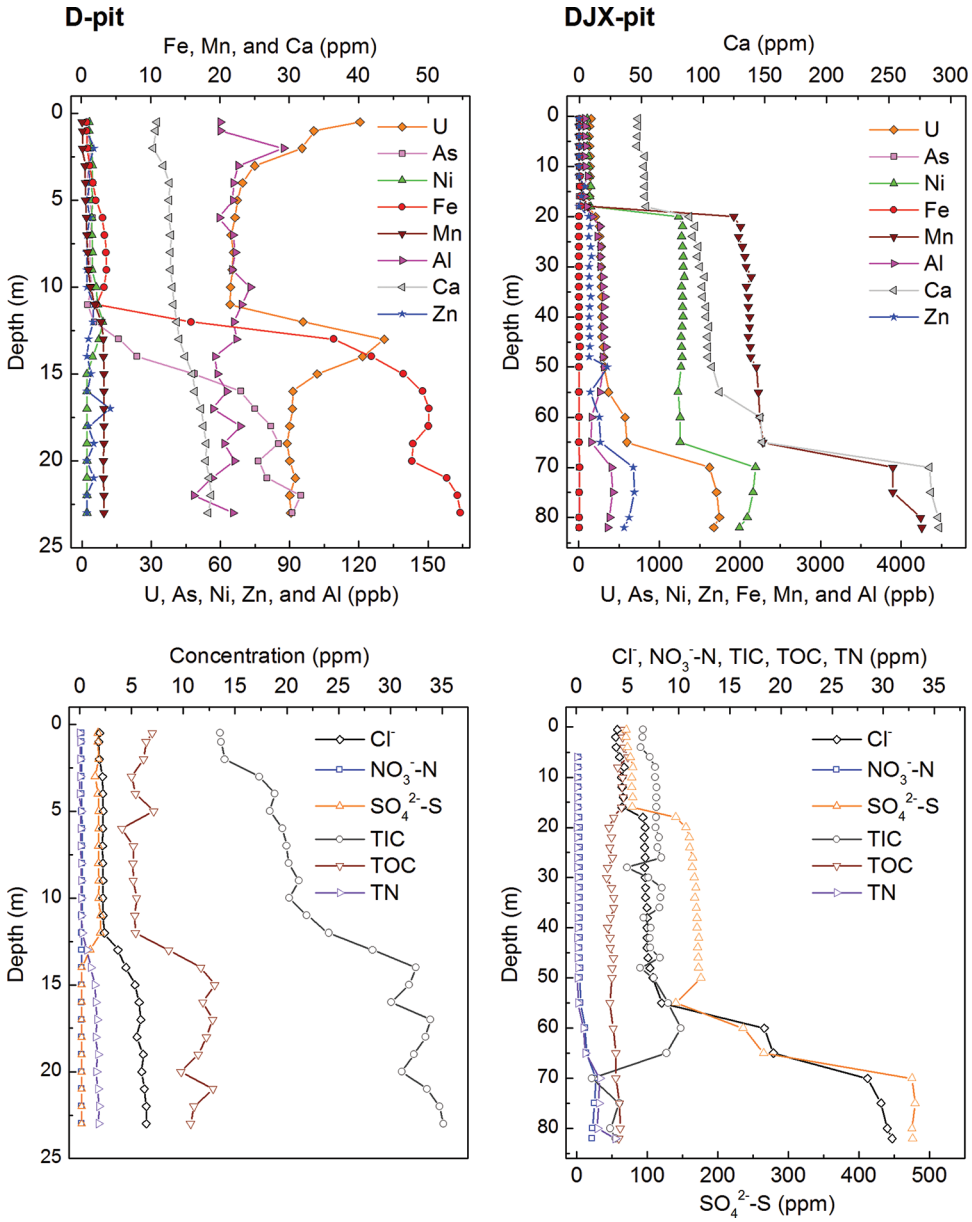

are nearly double those at the surface of the DJX pit (Table S12[1]). The lower chemocline (65 m) was sharp and was well developed for most metals in the DJX pit (exceptions: Li, Al, and Si). This lower zone could be due to remnant mine water from the time when the pit was used for temporary mine water storage prior to being flooded with freshwater from Cluff Lake. Arsenic and Fe concentrations were low (<2 ppb and <28 ppb, respectively) throughout the water column. Results for DJX pit obtained in September 2015 indicated higher Fe concentrations (4.6 ppm at 70 m, see Table S3[1]) compared with the June 2016 results (7 ppb), whereas Mn concentrations were marginally lower (3.6 ppm vs. 3.9 ppm at 70 m). Oxygen concentrations in the DJX pit were lower in September 2015 (personal communication, CanNorth), suggesting that the bottom of the DJX pit is not consistently oxygenated every year (see section 5.1).

Metal concentrations, anions, carbon, and nitrogen results for the three sampled groundwater wells are shown in Tables S5–S8[1]. A Piper diagram showing the water composition of these samples in relation to the pit water samples is shown in Fig. S6[1]. The well GW1, close to D pit, was rich in Na (2.2 ppm), Mg (7.2 ppm), and Ca (11.4 ppm), whereas the Fe concentration was only 0.5 ppm. Well GW2, located at the northern end of DJX pit, was rich in Na (125.9 ppm), Mg (49.5 ppm), K (12.5 ppm), and Ca (155.4 ppm), and had higher concentrations of Fe and Br compared with the pit water. GW3 had, in general, lower metal concentrations.

The relative abundance of Al, Fe, As, and Ni in the water columns of the two pits match well with the concentrations found in the adjacent rock samples (Section 3 in SI and Table S14[1]). Rock samples and the water in DJX pit had high concentrations of Al and Ni, whereas D pit rock samples and water were more enriched in Fe and As. Some elements, however, showed opposite trends, such as Zn, Mn, and U.

3.3. Speciation of metals

In D pit, Fe(II) concentrations increased with depth, with 78%–80% of total Fe as Fe(II) in deeper water layers (Table 1). The results for D pit demonstrate that there is a distinct shift in Fe speciation towards Fe(II) species below the depth where the ORP switches

Table 1. Fe(II) and total Fe concentration determined by the ferrozine absorption method in the D pit and the groundwater (GW1) well close to it.

Depth (m)	Total Fe (ppm)	Fe(II) (ppm)	Percent of total
0.5	n.d.	n.d.	—
5	0.92±0.31	0.09±0.13	9.7
10	1.26±0.54	0.28±0.22	22.7
15	52.25±2.21	41.83±1.02	80.1
20	51.59±2.69	40.02±1.60	77.6
GW1	0.93±0.06	0.29±0.03	31.4

Note: ppm, parts per million; n.d., not detected; GW1, DWW0041 G.

from positive to negative near 12 m. The groundwater close to D pit (GW1) was dominated by Fe(III), with only 31% Fe(II). In DJX pit, neither Fe(II) nor total Fe were detected by the ferrozine method, and only traces of Fe could be found using ICP-MS/MS. Water in well GW3, located west of the DJX pit, also had no detectable Fe.

IC-ICP-MS for D pit samples showed the abundance of As(III) and As(V). In general, the sum of As(III) and As(V) were close to the total As concentration at each depth (Table 2). A marked shift in As speciation was observed between depths of 10 m to 13 m. The high concentrations of As in the D pit below the chemocline are the result of the reducing conditions in the monimolimnion, which not only promote the reduction of Fe(III) but also the reduction and release of any bound As(V) species to the more mobile As(III) form. Arsenic speciation determination was problematic in the DJX pit due to the presence of unknown As species and their co-elution with known peaks at determined retention times.

Thermodynamic modeling with PHREEQC software showed a charge balance difference of >10% close to the D pit chemocline and below (Table S11[1]), indicating that not all charge bearing components were fully identified and modeled. For example, colloid-bound metals and organometallic species might have a strong influence due to their abundance and high surface charge. As shown in Table 3, the model predicted the dominant U(VI) species to be $UO_2(CO_3)_2^{2-}$ and $UO_2CO_3^0$ for the top 10 m of each pit. In D pit, at the chemocline and at 20 m depth, $U(OH)_5^-$ was expected to dominate, whereas in the DJX pit, $UO_2CO_3^0$, UO_2^{2+}, and $UO_2SO_4^0$ were predicted to become the dominant species in deeper layers. In the D pit, the saturation index was positive for U_4O_9, UO_2, and $USiO_4$ at and below the chemocline. In the DJX pit, U_3O_8 and U_4O_9 were saturated at 80 m depth. Precipitation of U(IV) species may explain the observed concentration drops in the D pit of U and Si below 13 m depth (Table S5[1]). Compared with IC-ICP-MS results, As(V) species were overestimated for the D pit surface water and underestimated for the deeper water layers. On the other hand, As(III) species were underestimated by the calculations above the chemocline at 13 m depth. $HAsO_4^{2-}$ and $H_2AsO_4^-$ were calculated to be the dominant As species in the DJX pit at all depths. Nickel was predicted to be predominately $NiCO_3^0$ in the D pit (up to 96%) and Ni^{2+} in the DJX pit (up to 80%), but in the DJX pit, due to high SO_4^{2-} concentrations, $NiSO_4^0$ (up to 28%) was also predicted.

3.4. Colloidal metal fractions

Colloidal fraction analyses for D pit indicated high variability with depth with regards to the distribution of metals between free ions, dissolved organic matter (DOM) and oxyhydroxide fractions (Tables S9 and S10[1]). For most of the metals investigated, the free ion phase was the dominant species. An exception was Al, which was predominantly in the DOM and oxyhydroxides size fractions, which may indicate the presence of colloidal aluminosilicates (Filella, 2006). This was particularly evident in D pit, where DOM contributed up to 67% (5 m) of the Al, whereas oxyhydroxide contributions made up the remaining 33% (0.5–5 m). In contrast, in the DJX pit the DOM size fraction (up to 59%) and the oxyhydroxide fraction (up to 23%) only played a role in Al partitioning in the surface waters (0.5–10 m).

Table 2. IC-ICP-MS results for As speciation in the D pit and total As based on iCAP Q ICP-MS.

	Total As	As(V)		As(III)	
Depth (m)	ppb	ppb	Percent of total	ppb	Percent of total
0.5	1.58	0.94	59.5	0.54	34.2
5	2.45	1.12	45.7	0.63	25.7
10	3.56	1.68	47.2	0.95	26.7
13	16.52	2.91	17.6	14.41	87.2
15	46.83	8.72	18.6	41.47	88.6
18	75.38	12.91	17.1	70.38	93.4
20	69.87	12.05	17.2	61.38	87.8
23	85.43	12.15	14.2	77.05	90.2

Note: IC, ion chromatograph; ICP-MS, inductively coupled plasma mass spectrometer; iCAP Q, quadrupole inductively coupled plasma mass spectrometer; ppb, parts per billion.

For U, Ni, and As, the colloidal distribution in the two pit lakes was different (Fig. 5). In the mixolimnion of the D pit, U was mostly associated with the oxyhydroxide size fraction (up to 12%), with a small contribution by DOM (up to 3%). At 0.5 m, 5 m, and 10 m, there was a progressive increase for U in the oxyhydroxide size fraction with 0%, 7%, and 12% being colloidal, respectively (Fig. 5). This fraction then dropped to 2% at the chemocline. This pattern was inversely related to the pH (Fig. 3) and U concentrations (Fig. 4) in the mixolimnion of the D pit. Nickel was scarce in the D pit water column; however, up to 34% of Ni in the mixolimnion and all Ni found at 20 m depth was in colloidal form (DOM). For As in the D pit, the oxyhydroxide size fraction played an important role, hosting up to 42% of the total As in the oxic water layers. Below the chemocline (13 m) As was mostly found as a free ion, suggesting that in contrast to U, As was not binding to reduced particulate organic matter.

In the DJX pit, colloidal U (associated with oxyhydroxides) was only relevant in the samples below the upper chemocline (>30 m) where it contributed approximately 16% of total U. The same colloidal material also carried minor amounts of Al (0.9–1.8 ppb), but no Fe or Mn (Table S10[1]), which might indicate that the U-bearing colloids were Al oxyhydroxides. Despite high (>2.1 ppm) Ni concentrations below 20 m depth of the DJX pit, colloidal Ni was only present above 30 m. At 0.5 m, Ni was bound to colloidal DOM (6%) and oxyhydroxides (33%). Below 10 m the colloidal Ni contribution was <1%, which might suggest that DOM-sized colloids are more important for Ni transport (as in D pit); however, those particles are respired in deeper layers of the oxygenated DJX pit. Arsenic concentrations were <1.5 ppb and colloidal As was only detected in the surface water sample (0.5 m), dominantly in the form of oxyhydroxides (9%).

Other metals that were largely represented in the oxyhydroxide fraction were Fe in the mixolimnia of the D pit (32%) and DJX pit (25%) and Co in the mixolimnion of the DJX pit (24%). Despite the high concentrations of Mn in both pit lakes, only the D pit showed the presence of colloidal Mn (up to 6%). Therefore, the observed oxyhydroxides are expected to contain mainly Al and some Fe (mostly D pit). The presence of such colloids was also predicted by PHREEQC calculations, which indicated oversaturation for mineral phases, including boehmite, diaspore, nontronite, and hematite (SI Appendix 1[1]).

3.5. Microbial communities

The relative distribution of phylogenetic classes, as determined by 16S rRNA gene sequencing, revealed a high microbial diversity within the two pit lakes (Fig. S8[1]). Qualitatively, the classes with the highest representation in the water column were Alphaproteo-

Table 3. PHREEQC modeling results for U, As, and Ni at selected depths.

			D pit					DJX pit		
Element	Oxidation state	Species	0.5 m	5 m	10 m	13 m	20 m	0.5 m	50 m	80 m
U	U(IV)	$U(OH)_5^-$	0%	0%	0%	98%	100%	0%	0%	0%
		$U(OH)_4$	0%	0%	0%	1%	0%	0%	0%	0%
	U(VI)	$UO_2(CO_3)_2^{2-}$	83%	34%	24%	0%	0%	71%	1%	0%
		UO_2CO_3	14%	65%	75%	0%	0%	26%	77%	56%
		$UO_2(CO_3)_3^{4-}$	3%	1%	0%	0%	0%	2%	0%	0%
		UO_2OH^+	0%	0%	0%	0%	0%	1%	6%	9%
		UO_2^{2+}	0%	0%	0%	0%	0%	0%	10%	17%
		UO_2SO_4	0%	0%	0%	0%	0%	0%	4%	11%
	Saturation indices	U_3O_8	−3.7	−4.6	−4.3	−3.0	−16.0	−1.3	−2.8	0.6
		U_4O_9	−6.4	−4.1	−3.1	14.3	4.3	−2.4	−3.7	1.7
		UO_2	−2.7	−1.7	−1.3	5.4	4.0	−1.6	−1.9	−0.4
		$USiO_4$	−3.7	−2.4	−2.0	4.8	3.3	−2.8	−2.5	−1.0
As	As(III)	H_3AsO_3	0%	0%	1%	100%	98%	0%	0%	0%
		$H_2AsO_3^-$	0%	0%	0%	0%	2%	0%	0%	0%
	As(V)	$HAsO_4^{2-}$	77%	32%	25%	0%	0%	77%	8%	10%
		$H_2AsO_4^-$	23%	68%	75%	0%	0%	23%	92%	90%
Ni		$NiCO_3$	79%	31%	22%	50%	96%	52%	0%	0%
		Ni^{2+}	19%	63%	72%	45%	4%	40%	80%	72%
		$NiHCO_3^+$	2%	5%	5%	5%	1%	2%	0%	0%
		$NiSO_4$	0%	0%	1%	0%	0%	6%	19%	28%

Note: The distribution of major calculated species (in %) and the saturation indices for solid species are shown. A similar table with molar concentrations can be found in the supplementary information (SI) (Table S11[1]). The full output can be found in SI Appendix 1[1].

Fig. 5. Colloidal distribution of dissolved, organic matter associated (DOM), and oxyhydroxide associated (Oxyhyd) U, Ni, and As in the D pit and DJX pit lakes. Distribution of other metals can be found in Tables S9 and S10[1]. Example fractograms for U, Ni, and As are presented in Fig. S7[1]. [Colour online.]

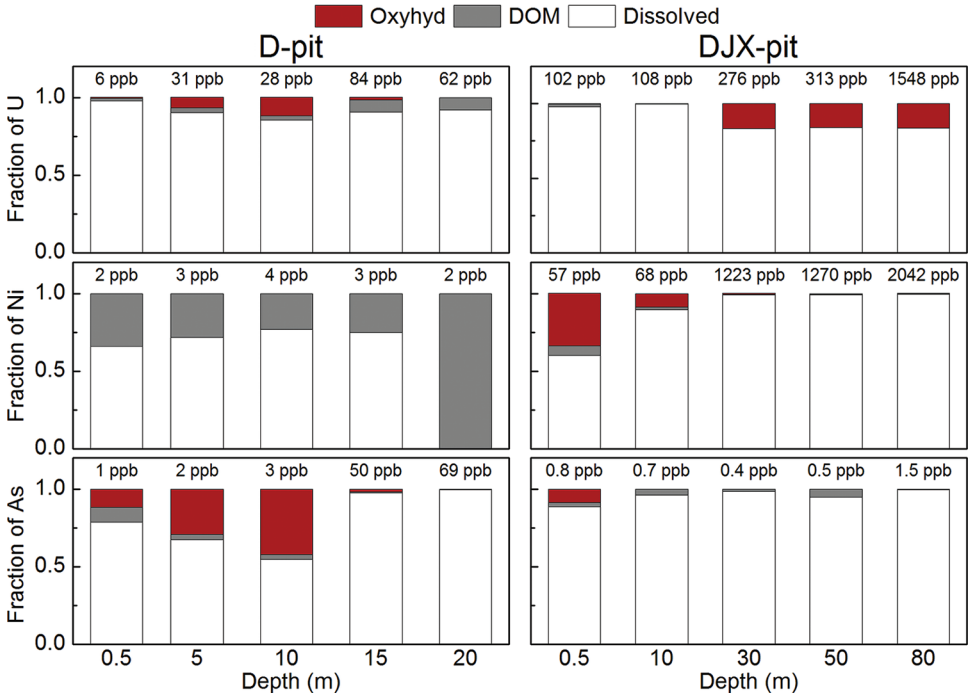

bacteria, Betaproteobacteria, Gammaproteobacteria, Actinobacteria, and Flavobacteria. Metal reduction studies in groundwater have suggested that Actinobacteria are most active at circumneutral pH and when NO_3^- is absent (Williams et al. 2013), which was the case for the two pit lakes. In the D pit, the classes Acidobacteria, Holophagae, and Acidimicrobia were found in greater abundance than in the DJX pit, whereas the latter showed a higher abundance of Sphingobacteria. The calculated Shannon diversity indices were highest close to the chemoclines in both pits (Fig. S9[1]). Specifically, the highest indices were found for D pit at 5 m depth (7.1), followed by DJX pit at 70 m (6.9), and D pit at 15 m (6.4). Lowest diversity indices were calculated for DJX pit at 20 m (5.0) and D pit at 0 m (4.6). The highest microbial diversity in the D pit was, therefore, linked to the thermocline around 5 m and the redox transition zone with the highest ORP gradient at 15 m. Similarly, in DJX pit, the diversity increase was related to the deep chemocline at 65 m. These findings are consistent with other authors (Falagán et al. 2013, 2014) that showed that highest diversity and abundance in meromictic lakes is linked to the chemoclines.

The dominant prokaryotic taxa are summarized in Table S13[1]. One of the most abundant species in both pits was a close relative to *Arthrobacter sp.*, an Mn(II)-oxidizing species that has been previ-

Fig. 6. Schematic summary of ongoing processes influencing the stratification and distribution of U in both pits. In the D pit (left) the Fe cycling drives the reduction and oxidation of U in the mixolimnion and at the chemocline, together with photosynthesis. Carbonate complexation in deeper water layers keep U(VI) in solution even under anoxic solutions. In the DJX pit (right) Ca cycling is the driving force behind the stratification and Al oxyhydroxides drive the accumulation of U in deeper water layers. [Colour online.]

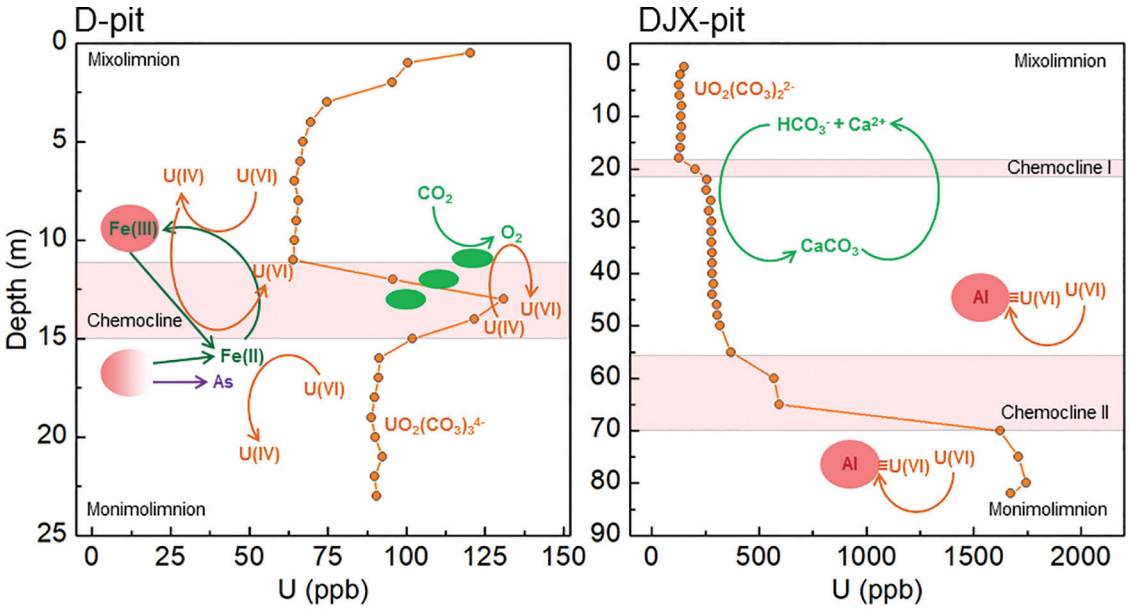

ously identified at uranium mine sites (Bohu et al. 2016). Its highest abundance was observed at 20 m depth of the DJX pit, where an increase in Mn concentrations from 0.1 ppm to over 2 ppm occurred. A close relative to another dominant species, *Alkaliphilus peptidifermentans strain Z-7036*, was particularly abundant at the depth of the thermocline. This spore-forming aerotolerant anaerobic organism is known to reduce Fe(III) (Zhilina et al. 2009). Microorganisms closely related to those associated with U(VI) reduction, such as *Desulfosporosinus orientis* (also SO_4^{2-} reducing), *Clostridium acetobutylicum, Geobacter uraniireducens*, *Geobacter metallireducens*, and *Geobacter sulfurreducens* (Williams et al. 2013) were also found in both pit lakes. Species of the named genera were previously shown to be stimulated during in situ U(VI) reduction experiments (e.g., Xu et al. 2010; Van Nostrand et al. 2011; Alessi et al. 2014). With the exception of the close relative to *Geobacter sulfurreducens*, the species discussed above were more abundant in D pit than DJX pit, especially close to the chemocline (10 m sample). *Geobacter uraniireducens* is mainly an Fe(III)-and Mn(IV)-reducing microorganism, which can grow at temperatures above 10 °C (Shelobolina et al. 2008). Its growth might be seasonally limited to the water layers above the thermoclines of the pits at 5 m (D pit) and 20 m (DJX pit), respectively. The pH range below 5 m depth may further limit growth, as *Geobacter uraniireducens* is best suited to pH conditions between 6.0 and 7.7. Despite those limitations, a microorganism most closely related to *Geobacter uraniireducens* was present in all water depths of both pit lakes. A bacterium related to *Geobacter metallireducens*, a strict anaerobic bacterium capable of reducing Fe(III), Mn(IV), and U(IV) (Lovley et al. 1993), was detected in deeper layers of the DJX pit (70 m) and D pit (15 m). Also capable of U(VI) reduction, *Desulfosporosinus orientis DSM 765* is a strictly anaerobic Gram-negative bacterium, that can grow chemoheterotrophically using SO_4^{2-} or thiosulfate as electron acceptors, or autotrophically with hydrogen and SO_4^{2-} (Stackebrandt et al. 1997). A close relative to this bacterium was less abundant in the DJX pit than the D pit, even with the higher concentrations of U and SO_4^{2-}, highlighting its preference for anoxic environments.

One Betaproteobacterium species was most closely related to *Rhodoferax ferrireducens*. This phototrophic bacterium was more abundant in D pit, especially at the chemocline, which was consistent with the concentrations of Fe(II) found in this pit. Another bacterium, which is often found with higher Fe concentrations is *Sideroxydans lithotrophicus*, is known to oxidize Fe(II) (Emerson and Moyer 1997); a close relative was abundant in deeper layers of the D pit where higher Fe concentrations prevailed. Bacteria possibly capable of As(III) oxidation were found in both pits, such as representatives of the genus *Rhizobium* (Campos et al. 2009; see SI Appendix 2[1]) or some *Pseudomonas* strains (Paul et al. 2014). A Betaproteobacterium most closely related to the As(III)-oxidizing bacterium *C05* was only found in the D pit and predominantly in the mixolimnion. Representatives of the previously described genera *Geobacter*, *Desulfosporosinus,* and additionally *Alkaliphilus,* are all capable of dissimilatory As(V) reduction (Giloteaux et al. 2013). Microorganisms from these genera were found in both pits, but they were more abundant in the zone close to the chemocline of the D pit.

4. Discussion

4.1. Geochemical metal cycling

In both pit lakes, meromixis influences the cycling of the major contaminants, especially U and As. Both pit lakes had pH >7 at the surface and were likely influenced by photosynthesis and CO_2 exchange with the atmosphere that can lead to strong carbonate complexation of U. Due to intrinsic acid generation from the surrounding waste rocks and aerobic respiration of organic materials, the pH dropped with increasing depth (Fig. 3). However, the sharp change in the ORP in the D pit prevented the acidification below the chemocline as a consequence of Fe(III) and SO_4^{2-} reduction, metabolisms that both lead to the generation of bicarbonate (Boehrer and Schultze 2008; Geller et al. 2012). Iron in general was one of the drivers for the stratification of the D pit (Boehrer and Schultze 2008; Boehrer et al. 2017). Additionally, this Fe cycling could be the key driver for U concentration changes in this pit, as summarized in Fig. 6. The Fe and U redox couples have similar potentials, and small changes in water chemistry can turn reducing agents into oxidizing agents (Du et al. 2011). For instance, Fe(II) could diffuse upwards through the chemocline to reduce U(VI) (Liger et al. 1999). This leads to U(IV) precipitates forming above

the chemocline, which could then drive down the total U concentration just above the chemocline. U(IV) precipitates might subsequently get oxidized back to soluble U(VI) by forming Fe(III)-bearing colloids, causing an increase in total U at 13 m depth; this is supported by oxygenic photosynthesis at this depth (Fig. S11[1]). Below the chemocline, alkaline conditions lead to strong carbonate complexation of U(VI), which was supported by the increasing total inorganic carbon concentrations (Fig. 4). Carbonate complexation prevents U(VI) from being reduced completely by Fe(II) and S(-II) (Anderson et al. 1989). The reductive dissolution of amorphous Fe(III) oxyhydroxides, and other Fe minerals in the D pit, release mineral-bound and co-precipitated As causing its concentrations to rise below 13 m depth. Reducing conditions also favored the formation of organic colloids that can contribute to the Ni and As transport (Fig. 5).

Colloids in the D pit might also contribute to U cycling by scavenging U(VI) from the water column. Indeed, speciation models for the mixolimnion predicted a decrease in negatively charged U(VI) species due the decreasing pH (Table 3). The anionic species, $UO_2(CO_3)_2^{2-}$ and $UO_2(CO_3)_3^{4-}$, are calculated to make up approximately 86% of all U species at 0.5 m. This fraction decreased to 35% at 5 m and 24% at 10 m, concomitant with the neutrally charged $UO_2CO_3^0$ becoming the dominant species. At a pH of 6.0–6.5, $UO_2CO_3^0$ is more likely to sorb to hydroxyl groups of the oxyhydroxide colloids, which can agglomerate to form larger particles and remove U from solution. At the chemocline, aqueous U(IV) was predicted to be present mostly as $U(OH)_5^-$. However, the abundance of Fe or Al oxyhydroxide colloids progressively decreased with depth, and in the monimonlimnion, DOM became the dominant U bearing colloidal phase (up to 8% of total U). In the D pit, the oxyhydoxides also played an important role for As, and hosted up to 42% of the total As in the mixolimnion (Fig. 5), which was likely due to As co-precipitation onto Fe oxyhydroxide particles (Slowey et al. 2007).

Meromixis in the DJX pit was predicted by Dessouki et al. (2005) who performed phosphate fertilization experiments in the pit before it was completely flooded. In the DJX pit no change in ORP was observed and the pH dropped to 5.5 after the first chemocline (Fig. 3). This pit illustrates a "stairs-like" meromixis type that could be influenced by Ca (Boehrer and Schultze 2008; Boehrer et al. 2017). The formation and precipitation of $CaCO_3$ in the upper 20 m, and its subsequent dissolution below the chemocline, might lead to the accumulation of Ca in deeper water layers, which further stabilized the stratification (Fig. 6). The DJX pit might also be influenced by Mn cycling (Boehrer and Schultze 2008; Boehrer et al. 2017). Mn(IV)-oxides could be precipitating in the well-oxygenated water but then get reduced to Mn(II) at the very bottom of the water column, inducing a rise of Mn concentrations that would increase stratification stability. A similar stairs-like meromixis was found in the Cueva de la Mora pit lake in Spain, which was not only due to double-diffusive convection processes but was likely also induced by sulfate- and metal-laden groundwater inputs entering the mine through intersecting galleries (Schultze et al. 2017). Al-bearing colloids could be responsible for additional U accumulation in deeper water layers (Fig. 5). Similarly, removal of As by precipitating Al oxyhydroxides was proposed by Sánchez-España et al. (2016) in the San Telmo acidic pit lake (Spain).

In general, because of the oxic conditions, colloidal transport of metals in the DJX pit was limited to oxyhydroxide particles. There are a number of potential hypotheses that may explain the presence of oxygen in the lower layers of DJX pit. For example, oxygen may still be present from the days of flooding, due to the low oxygen demand of deeper DJX pit layers, or there may be oxygenated groundwater inputs to the lower layers (Geller et al. 2012). Some of the wells located north of the DJX pit, lying in an area that is hydrologically upgradient of the pit, were tested in June 2017 and found to contain oxygen. Examples are wells shown in Fig. S1[1]: HYD07–11G (11.8 m deep) with 3.1 mg/L oxygen and HYD06–03G (5.0 m deep) with 3.5 mg/L oxygen. Additionally, the bedrock in the mining area is fractured and weathered (AREVA 2009), which may favor input of oxygenated groundwater. Therefore, the DJX pit may not truly be meromictic, since, under this scenario, renewal of the monimolimnion with oxygen-containing water is quite uncommon. Although groundwater inputs might destabilize the pit's stratification by reducing the salinity in the monimolimnion (Pieters and Lawrence 2014), the opposite appears to be the case in the DJX pit. The concentrations of SO_4^{2-}, Cl^-, B, Na, Ca, and Br found in the GW2 (Tables S6 and S8[1]), north of the DJX pit, suggests that higher salinity groundwater is moving from the north towards the DJX pit. This plume might be partially responsible for the chemocline at 65 m depth, bringing in not only the above mentioned anions and cations, but also Ni and U that had eluted from the waste rock in the backfilled DJN pit and the adjoining bedrock (Fig. 2). The observation of oxygen in the DJX pit might be explained by occasional mixing processes. The shallower portion of the pit, over the backfilled DJN, could be cooling faster in the winter causing this oxygenated water to slide down toward deeper layers and leading to episodic deep water renewal, a process previously observed in Lake Malawi (Boehrer and Schultze 2008). However, further investigations of the shallower portions of the pit would be needed to refine the understanding this and other potential sources of oxygen in the lower layers of the DJX pit.

The high relative depth of both pit lakes is likely a key contributor to their stable stratification (Pieters and Lawrence 2014). D pit and DJX-pit have relative depths of 20% and 27%, respectively, and formation of an ice cover every year promotes stable chemoclines in both pits. Factors that might disturb meromixis in the case of D pit and DJX pit are rock falls, landslides (Fig. S10[1]), surface water inputs, and potential changes in groundwater flow.

4.2. Microbial communities in comparison to acidic pit lakes

The overall microbial composition in the Cluff Lake pits was different from previously studied acidic (pH 2.5–4.5) pit lakes, such as Cueva de la Mora and Guadiana in Spain (Falagán et al. 2013, 2014). Bacteria dominant in those two lakes, including *Leptospirillum sp.*, *Acidithiobacillus sp.*, *Metallibacterium sp.*, *Thiomonas sp.*, and *Desulfomonile sp.*, were not detected in the Cluff Lake pits (SI Appendix 2[1]). Generally, compared to the acidic pit lakes, Acidobacteria and Deltaproteobacteria were less abundant in the Cluff Lake pits (Fig. S8[1]). On the other hand, bacteria reported to be related to *Desulfosporosinus sp.* (see above) were found, and they were more dominant in the pH-neutral D pit, likely due to the anoxic conditions found there (Falagán et al. 2014). Relatives of the acidophilic and aerobic bacterium *Alicyclobacillus sp.* (Chang and Kang 2004), which was previously identified in acidic pit lakes (Falagán et al. 2013, 2014) were also found at the chemocline of the D pit. Falagán et al. (2014) identified various archaea of the order Thermoplasmatales and the phyla Thaumarchaeota and Crenarchaeota in the acidic pit lakes. In this study, relatives of Thermoplasmates were identified mostly in the DJX pit and Thaumarchaeota were only detected in the water column of the D pit (SI Appendix 2[1]). Crenarchaeota were not detected in either of the pits.

4.3. Potential for enhanced remediation

The meromictic behavior of the investigated pit lakes opens potential opportunities by enhancing the use of pit lakes as a remediation strategy by promoting metal precipitation in the monimolimnia (Fisher and Lawrence 2006; Pieters and Lawrence 2014). For example, the application of fertilizer over longer time periods would enhance algal growth in the mixolimnion, which may lead to enhanced metal removal from this layer through metal sorption and uptake by algal cells, as demonstrated previously over a shorter term in the DJX pit by Dessouki et al. (2005). Fertilization with

phosphorus was observed to increase the removal of metals (e.g., U, Ni, Zn, Mn, Cu, As) from the surface water and their accumulation the sediments. Metal removal through fertilization was also achieved in the Island Copper Mine pit lake (Canada) through the addition of nitrogen and phosphorus (Schultze et al. 2017). An additional effect of fertilization could be the stimulation of sulfate-reducing bacteria (such as *Desulfosporosinus orientis*) in the monimolimnion, which would promote the formation of insoluble sulfide minerals, such as NiS, in the DJX pit. Arsenic sulfides might form and could lead to the coprecipitation of As(III) with ferrous sulfides in the D pit, as been seen in the Cueva de la Mora pit (Schultze et al. 2016). Similarly, in the Island Copper Mine pit lake, metal removal from the mixolimnion through the formation of sulfides at the chemocline was found to be an efficient process (Schultze et al. 2017).

The formation of insoluble sulfides might also lead to the development of a significant U sink, as sulfide particles can remove U from the water column though sorption (Wersin et al. 1994; Diez-Ercilla et al. 2014). Moreover, reducing conditions could promote the precipitation of U(IV) through *Desulfosporosinus orientis*, *Geobacter* species or other U(VI)-reducing organisms, when sufficient electron donors are available (Williams et al. 2013). Differing remediation approaches would likely be required between D pit and DJX pit, as their redox conditions vary considerably. The presence of oxygen in deeper layers of the DJX pit, if it persists, could influence remediation outcomes. The formation of anoxia in the DJX pit through fertilization could initiate the formation of sulfides and U(IV) precipitation, but they are likely to already take place in the D pit. In contrast, the addition of sulfate, e.g., as gypsum (Lueders and Friedrich 2002; Kijjanapanich et al. 2014), to D pit might provide an electron acceptor for SO_4^{2-} reducing bacteria, including those which are known to actively reduce U(VI). Additionally, iron sulfides (e.g., mackinawite) might form and abiotically reduce U(VI) (Bargar et al. 2013; Veeramani et al. 2013; Alessi et al. 2014). Although reducing conditions are known to increase the bioaccessibility of As, in the long term, precipitates such as orpiment (As_2S_3) and realgar (AsS) might partially remove As from the water column (SI Appendix 1[1]).

5. Conclusions

Our study provides new insights on the geochemical behavior of dissolved and colloidal metals in meromictic pit lakes in a subarctic climate. Meromixis was found to determine the metal distribution, speciation, and colloidal formation in the pit lakes at Cluff Lake. The redox state and mineral composition of the bedrocks of the pits have led to the formation of two types of stratification. Strong reducing conditions in the monimolimnion of the D-pit led to increased As concentrations (mostly As(III) species), but did not promote the precipitation of reduced U minerals, likely due to U stabilization by carbonate complexation. The chemocline of this pit is a highly dynamic zone, governed by the cycling of Fe. In contrast, the oxic conditions and high Ca and Mg concentrations in the DJX pit with a staircase-like stratification, led to low As concentrations in the water column and an accumulation of U and Ni at the pit bottom. In both pits the association of metals with colloidal particles could be observed. Potential U(VI)-reducing microorganisms were mostly found near the chemocline of the D pit and in deeper layers of the DJX pit, and some of those microorganisms are known to reduce As(V). Further investigations at the Cluff Lake mine pits should focus on the speciation and size distribution of contaminant bearing colloids, and the U, As, and Ni distribution and speciation in the sediments of the pit lakes.

Acknowledgements

This work was supported by Natural Sciences and Engineering Research Council of Canada (NSERC) Discovery grants to D.S.A. (RGPIN–04134) and K.O.K. (RGPIN–165831), by a 2015–2016 Ashley and Janet Cameron Research and Education Seed Fund grant to D.S.A., and by a 2016–2017 University of Alberta Northern Research Award to T.W. The authors would like to thank to AREVA Resources Canada and CanNorth for the provided data and samples, borrowed equipment, technical support, and in-kind contributions. The authors further appreciate the support provided by Chad Cuss and Alexandre Bagnoud, and would like to thank the two anonymous reviewers for their valuable suggestions and comments.

References

Alessi, D.S., Lezama-Pacheco, J.S., Janot, N., Suvorova, E.I., Cerrato, J.M., Giammar, D.E., et al. 2014. Speciation and reactivity of uranium products formed during in situ bioremediation in a shallow alluvial aquifer. Environmental Science & Technology, **48**(21): 12842–12850. doi:10.1021/es502701u. PMID:25265543.

Anderson, R.F., Fleisher, M.Q., and LeHuray, A.P. 1989. Concentration, oxidation state, and particulate flux of uranium in the Black Sea. Geochimica et Cosmochimica Acta, **53**(9): 2215–2224. doi:10.1016/0016-7037(89)90345-1.

AREVA. 2009. Cluff Lake project. Detailed decommissioning plan, version 2. AREVA Resources Canada Inc.

AREVA. 2013. Cluff lake project: 2012 annual report. AREVA Resources Canada Inc.

Bargar, J.R., Williams, K.H., Campbell, K.M., Long, P.E., Stubbs, J.E., Suvorova, E.I., et al. 2013. Uranium redox transition pathways in acetate-amended sediments. Proceedings of the National Academy of Sciences, **110**(12): 4506–4511. doi:10.1073/pnas.1219198110.

Bell, K. 1985. Geochronology of the Carswell area, northern Saskatchewan. *In* The Carswell Structure Uranium Deposits, Saskatchewan. Geological Association of Canada, Vol. 29, pp. 34–46.

Boehrer, B., and Schultze, M. 2008. Stratification of lakes. Reviews of Geophysics, **46**(2). doi:10.1029/2006RG000210.

Boehrer, B., von Rohden, C., and Schultze, M. 2017. Physical features of meromictic lakes: Stratification and circulation. *Edited by* R. Gulati, E. Zadereev, and A. Degermendzhi. *In* Ecology of meromictic lakes. Ecological Studies (Analysis and Synthesis), Vol. 228. Springer, Cham.

Bohu, T., Akob, D.M., Abratis, M., Lazar, C.S., and Küsel, K. 2016. Biological low-pH Mn(II) oxidation in a manganese deposit influenced by metal-rich groundwater. Applied and Environmental Microbiology, **82**(10): 3009–3021. doi:10.1128/AEM.03844-15. PMID:26969702.

Campos, V.L., Escalante, G., Yañez, J., Zaror, C.A., and Mondaca, M.A. 2009. Isolation of arsenite-oxidizing bacteria from a natural biofilm associated to volcanic rocks of Atacama Desert, Chile. Journal of Basic Microbiology, **49**(Suppl. S1): S93–S97. doi:10.1002/jobm.200900028.

Chang, S.S., and Kang, D.H. 2004. Alicyclobacillus spp. in the fruit juice industry: history, characteristics, and current isolation/detection procedures. Critical Reviews in Microbiology, **30**(2): 55–74. doi:10.1080/10408410490435089. PMID:15239380.

Church, C.D., Wilkin, R.T., Alpers, C.N., Rye, R.O., and McCleskey, R.B. 2007. Microbial sulfate reduction and metal attenuation in pH 4 acid mine water. Geochemical Transactions, **8**(1): 10. doi:10.1186/1467-4866-8-10. PMID:17956615.

Cuss, C.W., and Guéguen, C. 2012. Determination of relative molecular weights of fluorescent components in dissolved organic matter using asymmetrical flow field-flow fractionation and parallel factor analysis. Analytica Chimica Acta, **733**: 98–102. doi:10.1016/j.aca.2012.05.003. PMID:22704382.

Dai, M., Martin, J.-M., and Cauwet, G. 1995. The significant role of colloids in the transport and transformation of organic carbon and associated trace metals (cd, cu and ni) in the Rhône delta (France). Marine Chemistry, **51**(2): 159–175. doi:10.1016/0304-4203(95)00051-R.

Dessouki, T.C.E., Hudson, J.J., Neal, B.R., and Bogard, M.J. 2005. The effects of phosphorus additions on the sedimentation of contaminants in a uranium mine pit-lake. Water Research, **39**(13): 3055–3061. doi:10.1016/j.watres.2005.05.009. PMID:15979684.

Diez-Ercilla, M., Sánchez-España, J., Yusta, I., Wendt-Potthoff, K., and Koschorreck, M. 2014. Formation of biogenic sulphides in the water column of an acidic pit lake: biogeochemical controls and effects on trace metal dynamics. Biogeochemistry, **121**(3): 519–536. doi:10.1007/s10533-014-0020-0.

Donahue, R., Hendry, M.J., and Landine, P. 2000. Distribution of arsenic and nickel in uranium mill tailings, Rabbit Lake, Saskatchewan, Canada. Applied Geochemistry, **15**(8): 1097–1119. doi:10.1016/S0883-2927(99)00114-6.

Donner, M.W., Javed, M.B., Shotyk, W., Francesconi, K.A., and Siddique, T. 2017. Arsenic speciation in the lower Athabasca River watershed: a geochemical investigation of the dissolved and particulate phases. Environmental Pollution, **224**: 265–274. doi:10.1016/j.envpol.2017.02.004. PMID:28216136.

Du, X., Boonchayaanant, B., Wu, W.-M., Fendorf, S., Bargar, J., and Criddle, C.S. 2011. Reduction of uranium (VI) by soluble iron (II) conforms with thermodynamic predictions. Environmental Science & Technology, **45**(11): 4718–4725. doi:10.1021/es2006012. PMID:21553877.

Emerson, D., and Moyer, C. 1997. Isolation and characterization of novel iron-oxidizing bacteria that grow at circumneutral pH. Applied and Environmental Microbiology, **63**(12): 4784–4792. PMID:9406396.

Falagán, C., Sánchez-España, F.J., and Johnson, D.B. 2013. Microbiological communities in two acidic mine pit lakes in the Iberian Pyrite Belt (IPB), Spain. Advanced Materials Research, **825**: 19–22. doi:10.4028/www.scientific.net/AMR.825.19.

Falagán, C., Sánchez-España, J., and Johnson, D.B. 2014. New insights into the biogeochemistry of extremely acidic environments revealed by a combined cultivation-based and culture-independent study of two stratified pit lakes. FEMS microbiology ecology, **87**(1): 231–243. doi:10.1111/1574-6941.12218. PMID: 24102574.

Filella, M. 2006. Colloidal properties of submicron particles in natural waters. *In* Environmental colloids and particles: Behaviour, separation and characterization. *Edited by* K.J. Wilkinson and J.R. Lead. Vol. 10. John Wiley & Sons, Ltd, Chichester, UK.

Fisher, T.S., and Lawrence, G.A. 2006. Treatment of acid rock drainage in a meromictic mine pit lake. Journal of Environmental Engineering, **132**(4): 515–526. doi:10.1061/(ASCE)0733-9372(2006)132:4(515).

Geller, W., Schultze, M., Kleinmann, B., and Wolkersdorfer, C. 2012. Acidic pit lakes: the legacy of coal and metal surface mines. Springer Science & Business Media.

Giloteaux, L., Holmes, D.E., Williams, K.H., Wrighton, K.C., Wilkins, M.J., Montgomery, A.P., et al. 2013. Characterization and transcription of arsenic respiration and resistance genes during in situ uranium bioremediation. The ISME Journal, **7**(2): 370–383. doi:10.1038/ismej.2012.109. PMID:23038171.

Guéguen, C., and Cuss, C.W. 2011. Characterization of aquatic dissolved organic matter by asymmetrical flow field-flow fractionation coupled to UV-visible diode array and excitation emission matrix fluorescence. Journal of Chromatography A, **1218**(27): 4188–4198. doi:10.1016/j.chroma.2010.12.038. PMID: 21227433.

Harper, C.T. 1981. Geology of the Carswell Structure, central part. Saskatchewan Geological Survey Report 214. Available from publications.gov.sk.ca/documents/310/90719-Report-214_Geology_Of_The_Carswell_Structure-Central_Part.pdf [accessed December 2016].

Jaeger, D. 1994. Effects of hypolimnetic water aeration and iron-phosphate precipitation on the trophic level of Lake Krupunder. Hydrobiologia, **275**(1): 433–444.

Kijjanapanich, P., Annachhatre, A.P., Esposito, G., and Lens, P.N. 2014. Use of organic substrates as electron donors for biological sulfate reduction in gypsiferous mine soils from Nakhon Si Thammarat (Thailand). Chemosphere, **101**: 1–7. doi:10.1016/j.chemosphere.2013.11.026. PMID:24332728.

Kozich, J.J., Westcott, S.L., Baxter, N.T., Highlander, S.K., and Schloss, P.D. 2013. Development of a dual-index sequencing strategy and curation pipeline for analyzing amplicon sequence data on the MiSeq Illumina sequencing platform. Applied and environmental microbiology, **79**(17): 5112–5120. doi:10.1128/AEM.01043-13.

Kretzschmar, R., and Schäfer, T. 2005. Metal retention and transport on colloidal particles in the environment. Elements, **1**(4): 205–210. doi:10.2113/gselements.1.4.205.

Kyser, K., and Cuney, M. 2008. Unconformity-related uranium deposits. Mineralogical Association of Canada. Short Course Series, Vol. 39, Mineralogical Association of Canada, Que., pp. 7–95.

Leigh, M.B., Wu, W.M., Cardenas, E., Uhlik, O., Carroll, S., Gentry, T., et al. 2015. Microbial communities biostimulated by ethanol during uranium (VI) bioremediation in contaminated sediment as shown by stable isotope probing. Frontiers of Environmental Science & Engineering, **9**(3): 453–464. doi:10.1007/s11783-014-0721-6.

Liger, E., Charlet, L., and van Cappellen, P. 1999. Surface catalysis of uranium (VI) reduction by iron (II). Geochimica et Cosmochimica Acta, **63**(19): 2939–2955. doi:10.1016/S0016-7037(99)00265-3.

Lovley, D.R., Giovannoni, S.J., White, D.C., Champine, J.E., Phillips, E.J.P., Gorby, Y.A., and Goodwin, S. 1993. Geobacter metallireducens gen. nov. sp. nov., a microorganism capable of coupling the complete oxidation of organic compounds to the reduction of iron and other metals. Archives of Microbiology, **159**(4): 336–344. doi:10.1007/BF00290916.

Lueders, T., and Friedrich, M.W. 2002. Effects of amendment with ferrihydrite and gypsum on the structure and activity of methanogenic populations in rice field soil. Applied and Environmental Microbiology, **68**(5): 2484–2494. doi:10.1128/AEM.68.5.2484-2494.2002. PMID:11976125.

Neubauer, E., von der Kammer, F., and Hofmann, T. 2013. Using flowfff and hpsec to determine trace metal-colloid associations in wetland runoff. Water Research, **47**(8): 2757–2769. doi:10.1016/j.watres.2013.02.030. PMID:23528782.

Paul, D., Poddar, S., and Sar, P. 2014. Characterization of arsenite-oxidizing bacteria isolated from arsenic-contaminated groundwater of west Bengal. Journal of Environmental Science and Health, Part A, **49**(13): 1481–1492. doi:10.1080/10934529.2014.937162.

Pieters, R., and Lawrence, G.A. 2014. Physical processes and meromixis in pit lakes subject to ice cover. Canadian Journal of Civil Engineering, **41**(6): 569–578. doi:10.1139/cjce-2012-0132.

Porsch, K., and Kappler, A. 2011. FeII oxidation by molecular O2 during HCl extraction. Environmental Chemistry, **8**(2): 190–197. doi:10.1071/EN10125.

Ruhlmann, F. 1985. Mineralogy and metallogeny of uraniferous occurrences in the Carswell structure: in the Carswell structure uranium deposits, Saskatchewan. Geological Association of Canada, Vol. 29, pp. 105–120.

Sánchez-España, J., Yusta, I., Gray, J., and Burgos, W.D. 2016. Geochemistry of dissolved aluminum at low pH: Extent and significance of Al–Fe (III) coprecipitation below pH 4.0. Geochimica et Cosmochimica Acta, **175**: 128–149. doi:10.1016/j.gca.2015.10.035.

Schultze, M., Castendyk, D., Wendt-Potthoff, K., Sánchez-España, J., and Boehrer, B. 2016. On the relevance of meromixis in mine pit lakes - an update. *In* Proceedings IMWA 2016 Annual Conference, Freiberg, Germany. Available from www.imwa.info/docs/imwa_2016/IMWA2016_Schultze_27.pdf [accessed December 2016].

Schultze, M., Boehrer, B., Wendt-Potthoff, K., Sánchez-España, J., and Castendyk, D. 2017. Meromictic pit lakes: Case studies from Spain, Germany and Canada and general aspects of management and modelling. *Edited by* R. Gulati, E. Zadereev, and A. Degermendzhi. *In* Ecology of meromictic lakes. Ecological Studies (Analysis and Synthesis), Vol. 228, Springer, Cham.

Schüring, J., Schulz, H.D., Fischer, W.R., Böttcher, J., and Duijnisveld, W.H. 2013. Redox: fundamentals, processes and applications. Springer Science & Business Media.

Shelobolina, E.S., Vrionis, H.A., Findlay, R.H., and Lovley, D.R. 2008. Geobacter uraniireducens sp. nov., isolated from subsurface sediment undergoing uranium bioremediation. International Journal of Systematic and Evolutionary Microbiology, **58**(5): 1075–1078. PMID:18450691.

Slowey, A.J., Johnson, S.B., Newville, M., and Brown, G.E. 2007. Speciation and colloid transport of arsenic from mine tailings. Applied Geochemistry, **22**(9): 1884–1898. doi:10.1016/j.apgeochem.2007.03.053.

Sobolewski, A. 1999. A review of processes responsible for metal removal in wetlands treating contaminated mine drainage. International Journal of Phytoremediation, **1**(1): 19–51. doi:10.1080/15226519908500003.

Stackebrandt, E., Sproer, C., Rainey, F.A., Burghardt, J., Päuker, O., and Hippe, H. 1997. Phylogenetic analysis of the genus Desulfotomaculum: evidence for the misclassification of Desulfotomaculum guttoideum and description of Desulfotomaculum orientis as Desulfosporosinus orientis gen. nov., comb. nov. International Journal of Systematic and Evolutionary Microbiology, **47**(4): 1134–1139.

Stookey, L.L. 1970. Ferrozine—a new spectrophotometric reagent for iron. Analytical Chemistry, **42**(7): 779–781. doi:10.1021/ac60289a016.

Vail, J. 2013. Groundwater sampling. Operating procedure. U.S. Environmental Protection Agency Science and Ecosystem Support Division. Athens, Georgia. Available from www.epa.gov/sites/production/files/2015-06/documents/Groundwater-Sampling.pdf [accessed June 2017].

Van Nostrand, J.D., Wu, L., Wu, W.M., Huang, Z., Gentry, T.J., Deng, Y., et al. 2011. Dynamics of microbial community composition and function during in situ bioremediation of a uranium-contaminated aquifer. Applied and Environmental Microbiology, **77**(11): 3860–3869. doi:10.1128/AEM.01981-10. PMID: 21498771.

Veeramani, H., Scheinost, A.C., Monsegue, N., Qafoku, N.P., Kukkadapu, R., Newville, M., et al. 2013. Abiotic reductive immobilization of U (VI) by biogenic mackinawite. Environmental Science & Technology, **47**(5): 2361–2369. doi:10.1021/es304025x. PMID:23373896.

Viollier, E., Inglett, P.W., Hunter, K., Roychoudhury, A.N., and van Cappellen, P. 2000. The ferrozine method revisited: Fe(II)/Fe(III) determination in natural waters. Applied Geochemistry, **15**(6): 785–790. doi:10.1016/S0883-2927(99)00097-9.

Wang, Y., Frutschi, M., Suvorova, E., Phrommavanh, V., Descostes, M., Osman, A.A., et al. 2013. Mobile uranium (IV)-bearing colloids in a mining-impacted wetland. Nature Communications, **4**. doi:10.1038/ncomms3942.

Watson, D.B., Wu, W.M., Mehlhorn, T., Tang, G., Earles, J., Lowe, K., et al. 2013. In situ bioremediation of uranium with emulsified vegetable oil as the electron donor. Environmental Science & Technology, **47**(12): 6440–6448. doi:10.1021/es3033555. PMID:23697787.

Wersin, P., Hochella, M.F., Persson, P., Redden, G., Leckie, J.O., and Harris, D.W. 1994. Interaction between aqueous uranium (VI) and sulfide minerals: spectroscopic evidence for sorption and reduction. Geochimica et Cosmochimica Acta, **58**(13): 2829–2843. doi:10.1016/0016-7037(94)90117-1.

Williams, K.H., Long, P.E., Davis, J.A., Wilkins, M.J., N'Guessan, A.L., Steefel, C.I., et al. 2011. Acetate availability and its influence on sustainable bioremediation of uranium-contaminated groundwater. Geomicrobiology Journal, **28**(5–6): 519–539. doi:10.1080/01490451.2010.520074.

Williams, K.H., Bargar, J.R., Lloyd, J.R., and Lovley, D.R. 2013. Bioremediation of uranium-contaminated groundwater: a systems approach to subsurface biogeochemistry. Current Opinion in Biotechnology, **24**(3): 489–497. doi:10.1016/j.copbio.2012.10.008. PMID:23159488.

Xu, M., Wu, W.M., Wu, L., He, Z., van Nostrand, J.D., Deng, Y., et al. 2010. Responses of microbial community functional structures to pilot-scale uranium in situ bioremediation. The ISME Journal, **4**(8): 1060–1070. doi:10.1038/ismej.2010.31. PMID:20237512.

Zhilina, T.N., Zavarzina, D.G., Kolganova, T.V., Lysenko, A.M., and Tourova, T.P. 2009. Alkaliphilus peptidofermentans sp. nov., a new alkaliphilic bacterial soda lake isolate capable of peptide fermentation and Fe (III) reduction. Microbiology, **78**(4): 445–454.